Journal of Power Sources 238 (2013) 435–441

Contents lists available at SciVerse ScienceDirect

Journal of Power Sources

journal homepage: www.elsevier.com/locate/jpowsour

Solid polymer electrolyte coating from a bifunctional monomer for three-dimensional microbattery applications

Bing Sun, I-Ying Liao, Semra Tan, Tim Bowden, Daniel Brandell*

Department of Chemistry – Ångström Laboratory, Uppsala University, Box 538, SE-75121 Uppsala, Sweden

HIGHLIGHTS

- A novel bifunctional monomer is synthesized.
- A cross-linked polymer electrolyte is produced from the monomer.
- The electrolyte shows functionality for Li-ion 3D-microbatteries.
- The material is electrochemically characterized.
- Functionality in Li-cells is demonstrated.

ARTICLE INFO

Article history:
Received 13 September 2012
Received in revised form
9 April 2013
Accepted 12 April 2013
Available online 19 April 2013

Keywords:
3D-microbattery solid electrolyte
Polymer electrolyte
Bifunctional monomer
Polyetheramine

ABSTRACT

This work comprises the synthesis and characterization of a novel solid polymer electrolyte based on oligomeric polyetheramine substituted with a methacrylic group at one of its three chain ends. This modification introduces a bifunctionality to the PEA monomer – it can act both as polymerizable unit and surfactant. Thin and pinhole-free polymer electrolyte layers could be constructed with thicknesses in the order of <1 μm using UV-initiated polymerization. The electrolyte exhibits good electrochemical and chemical stability up to 4 V vs. Li^+/Li. $LiFePO_4$ cathode coated with the electrolyte was cycled against lithium at 60 °C, and displayed reasonable capacity values ($\sim$140 mAh g^{-1}) for 10 cycles, where after Li dendrite formation contributed to battery instabilities.

1. Introduction

Three-dimensional microbatteries (3DMBs) open up new possibilities for small-scale energy storage solutions which can meet the combined demand of both high power and energy density [1,2]. In parallel to the development of new 3D-nanoarchitectured electrodes, it also becomes necessary to find a suitable electrolyte medium which is ion-conducting and electron-insulating, conformal and pinhole-free, and yet mechanically and electrochemically stable [1].

A handful of electrolyte systems have been explored for 3DMBs. Building on experiences from thin-film Li-ion batteries, primarily liquid or gel electrolytes have been applied to ensure sufficient ionic conduction and contacts at the electrolyte/electrode interfaces [3–6]. However, the liquid components introduce a limitation in flexibility and mechanical stability in the battery architectures. The flammable liquid components also bring risks of leakage and thermal runaway. Compared to conventional liquid electrolytes, solid polymer electrolytes (SPEs) provide improved safety and flexibility for various architectures and electrode materials. One of the most promising architectures of 3DMBs under development uses well-structured 3D arrays of nano-pillars or nano-rods as current collector, with deposition of active electrode materials on top of it [1,7–9]. A subsequent conformally deposited and ionically conductive polymer layer onto these structures would provide a significant step further toward finalization of the 3DMB. The energy and power density for this battery system depends on the amount of active materials deposited, as well as the thickness and conformal nature in the coating of the electrolyte.

It has previously been presented that the oligomer poly(ether amine) (glyceryl poly(oxypropylene); PEA), which has surfactant properties, can be blended within a cross-linked network of poly(-propylene glycol) diacrylate (PPGDA) to form uniform electrolyte coatings onto complex surfaces of electrodes [10], for the potential use in 3DMBs. The electrolyte could be solution-casted and then

* Corresponding author.
E-mail address: daniel.brandell@kemi.uu.se (D. Brandell).

0378-7753/$ – see front matter © 2013 Elsevier B.V. All rights reserved.
http://dx.doi.org/10.1016/j.jpowsour.2013.04.058

cross-linked to form a conformal SPE layer with thickness of a couple of microns. It displayed a stable electrochemical performance in 2D-$LiFePO_4$/SPE/Li thin film batteries at elevated temperature for over 30 cycles [11], and also showed functionality with nano-rod anodes of Cu_2Sb [11,12]. However, it still remains a challenge to form conformal and pinhole-free SPEs with controllable ultra-thin thickness in the order of sub-micron and nano-scale dimension. There is also great demand for SPEs with good chemical stability, to make further deposition of electrode active materials in all-solid-state Li-ion microbatteries viable [2,12].

The research presented here focuses on the synthesis and characterization of a novel solid polymer electrolyte consisting of PEA substituted statistically on average with one methacrylic group at one of its three oligomer chain ends. As a replacement to the blended PEA/PPGDA electrolyte system [10–12], this modification introduces a bifunctionality of the PEA monomer – it becomes both polymerizable and a surfactant. Considering that a fraction of the monomer will contain more than one acrylate end-groups after synthesis, they are also likely to form a cross-linked network after polymerization. Since the PEA oligomers are not covalently bonded to the cross-linked PPGDA network in the blend previously used, SPEs based on PEA/PPGDA are prone to dissolution in many common solvents (*e.g.*, ethanol and N-methyl-2-pyrrolidone, *etc.*). On the other hand, SPEs based on the substituted PEA can form strengthened network through polymerization of all monomeric units, thereby providing potential for further deposition of electrode materials in all-solid-state 3DMBs. Electrochemical and thermal properties of SPEs containing substituted PEA and LiTFSI at Li:O molar ratio of 1:20 are investigated. Pinhole-tests are also applied to analyze the ultra-thin SPE layer prepared by UV-initiated polymerization. Conformal and ultra-thin SPE layers were deposited on roughly structured $LiFePO_4$ cathodes and cycled against metallic lithium at elevated temperature.

2. Experimental

2.1. Chemicals

All chemicals for monomer synthesis, glyceryl poly(oxypropylene) triamine (PEA) (commercially named Jeffamine T-3000, Mn = 3000 g mol^{-1}, Huntsman), methacrylic anhydride (MAA) (Sigma–Aldrich, 94%), triethylamine (TEA) (Lancaster, 99%) and tetrahydrofuran (THF, Sigma–Aldrich, max 0.005% H_2O) solvent were used as received. Ethanol (Solveco, 99.5%) and Al_2O_3 (basic, Sigma–Aldrich) were utilized to remove by-product after synthesis. In the NMR analysis, deuterated dimethylsulfoxide (DMSO) (Sigma–Aldrich, 99.96 atom % D) was used as standard solvent. Lithium bis(trifluoromethane)sulfonylimide (LiTFSI) salt was purchased from Purolyte and used for producing polymer electrolyte. Phostech Lithium $LiFePO_4$ (with 2 wt.% carbon coating), poly(vinylidene fluoride) (PVdF, Fluka) and carbon black (ERACHEM) were mixed with n-methyl pyrrolidone (NMP) (VMR, 99.5%) for electrode preparation. KCl (VMR, 99.6%), $K_3Fe(CN)_6$ (C.P Bakers, 99.3%), acetonitrile (ACN) (Sigma–Aldrich, anhydrous, 99.8%), ferrocene (Sigma–Aldrich, 98%) and tetrabutylammonium perchlorate (TBAP) (Fluka, ≥99.0%) was used for pinhole tests. Polypropylene glycol diacrylate (PPGDA; Mn. ca 900, Sigma–Aldrich) was introduced for comparative experiments.

2.2. Synthesis and characterization of bifunctional monomers

Scheme 1 below illustrates the possible reaction route of the modified PEA monomer. It should be noted that besides the possible substitution of two or three of the amine groups on PEA, there are also possibilities to form imides in the reaction, which also could contribute to cross-linking the polymerized system. 20 g PEA was first dissolved in 10 ml THF. A mixture of 1 g MAA and 1 g TEA in 2 ml THF was then added dropwise into PEA solution. The molar ratio of PEA:MAA:TEA was kept as 1:1:1.5, thereby ensuring a statistical distribution of one substituent per oligomer. During the reaction, inert gas atmosphere was ensured to avoid exposure to moisture in air. After vigorous stirring of all reactants for 2 h, the resulting solution was heated at 50 °C using a rotary evaporator under vacuum to remove THF, and then dissolved in ethanol to remove a methacrylic acid by-product. The mixture was filtered through an Al_2O_3 column until no traces of the by-product could be detected in ^1H NMR. The final product was obtained after centrifugation of solid impurities and drying under vacuum for at least 12 h at 40 °C.

ATR-FTIR spectra were recorded before and after the substitution reaction on a Perkin–Elmer 983 IR spectrophotometer equipped with a ZnSe crystal. A resolution of 4 cm^{-1} was used for all samples and each spectrum was accumulated for 4 times within the wavenumber range of 4000–400 cm^{-1} at room temperature. Found peaks: 2850–2960 cm^{-1} (C–H stretching in the $-CH_2$ and $-CH_3$), 1900–2400 cm^{-1} (ZnSe crystal), 1620–1670 cm^{-1} (C=C stretching), 1500–1560 cm^{-1} (N–H bending coupled to C=O stretching), 1340–1470 cm^{-1} (the deformations of $-CH_2$ and $-CH_3$), 1399 cm^{-1} (=C–H bending), 1294 and 1258 cm^{-1} (C–O–C stretching), 1063 cm^{-1}(C–N stretching), 1102 cm^{-1} (C–O stretching), 660–900 cm^{-1} (NH_2 and N–H wagging).

NMR was also applied to confirm the substitution of the methacrylic group after synthesis, using a JEOL ECP-400 MHz NMR spectrometer with the proton signal of DMSO as internal standard. Each sample was scanned for 16 times for every data collection. ^1H NMR (DMSO-d_6) δ: 7.50 (N*H*CO, peak 2), 5.62 and 5.30 (H_2C=C(CH_3), peak 1), 3.50 and 4.12 (C*H*(CH_3)CH_2O, peak 5 and 5′), 3.30 (CH(CH_3)CH_2O, peak 6), 1.80 (CH_3C=CH_2, peak 3), 1.12 and 1.05 (CH(CH_3)CH_2O, peak 4 and 4′). All assignments of the PEA protons are illustrated in Fig. 2 (discussed below). Signals at 3.5 ppm and 4.3 ppm correspond to residuals of ethanol solvent.

The glass-transition temperature (T_g) of the synthetic monomer before and after UV-induced polymerization was probed by a Mettler Toledo DSC300. The samples within a weight range of 5–10 mg were sealed in aluminum pans. Each sample was first cooled down to −100 °C and then kept isothermal for 5 min. Afterward, the thermal properties of the sample were recorded during the heating process to 100 °C at a rate of 5 °C min^{-1}.

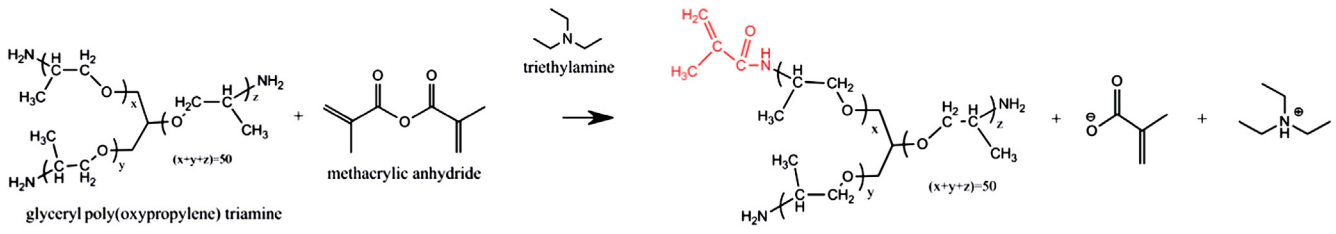

Scheme 1. Substitution of methacrylic groups on PEA.

LEO 1550 EG high resolution SEM was used to analyze the morphology of SPE-coated electrodes. A Polaron SC7640 Sputter coater with Au–Pd target was applied for gold coating to support imaging.

2.3. Preparation of polymer electrolyte

The as-prepared bifunctional monomer was mixed with LiTFSI at a Li:O molar ratio of 1:20 and 1 wt.% Irgacure 2022 in ethanol. The LiTFSI salt was dried in a vacuum oven at 120 °C for 24 h before usage. The homogenous solution was solution-casted onto standard $LiFePO_4$ composite electrodes. Ethanol was evaporated in vacuum at least 3 h and *in-situ* UV-initiated polymerization was then applied using a 160 W UV lamp at 365 nm for 2 min. All preparations were operated in a glove box filled with argon gas.

2.4. Electrochemical characterization

The ionic conductivity of the polymerized electrolytes was measured using symmetric stainless-steel electrodes with a diameter of 1.8 cm at AC $V_{rms} = 1$ V between 1×10^7 Hz and 1×10^{-2} Hz on a Solartron SI 1260 Impedance/Gain Phase Analyzer. The monomer solution was poured into a symmetric cell separated by a Teflon ring. In-situ UV-initiated polymerization was applied as described in Section 2.3 after removing ethanol solvent. Self-standing polymer membranes with a thickness of 3.1 mm were prepared by drying the whole setup in a vacuum oven at 40 °C for at least 2 h to remove the solvent.

Galvanostatical cycling using a Digatron BTS-600 was operated on a 'coffee-bag' cell at elevated temperature. $LiFePO_4$ electrodes were prepared by mixing 75% active material, 10% super P carbon black and 15% PVdF and casting on an aluminum foil. The electrodes were dried in a vacuum oven for at least 6 h at 120 °C before cell assembly. Batteries were cycled at different charge/discharge rates (C/25 and C/50) between 2.7 V and 4.2 V at 60 °C.

Cyclic voltammetry was conducted to determine both the electrochemical stability and the existence of pinholes in the polymer films. The electrochemical stability window was analyzed on a Bio-Logic VMP2 with a two-electrode setup using a lithium reference electrode and a nickel counter electrode at room temperature. The surface area of the electrode was 0.95 cm^2. SPEs prepared using substituted PEA were tested in comparison with unsubstituted PEA containing LiTFSI within a voltage window from −1.5–6.0 V with a scan rate of 5 mV s^{-1}. PEA/LiTFSI samples were prepared by soaking a glass fiber separator with PEA/LiTFSI solution. Thick free-standing SPEs containing substituted PEA and LiTFSI were prepared in the same way as for the ionic conductivity measurement. All samples were prepared in an argon-filled glove box.

Conducting fluorine-tin-oxide (FTO) glass ($R_s = 15\ \Omega$) was used as substrate for pinhole test. The monomer solution was first spin-coated onto the substrate and then polymerized after drying in vacuum. Three-electrode cyclic voltammetry was carried out in an aqueous solution of 0.1 M KCl with Pt auxiliary and SSCE-reference electrode. The electrode was scanned between −250 mV and 650 mV for 1 mM $Fe(CN)_6^{3-}$ at a scan rate of 100 mV s^{-1}. Pinhole test in nonaqueous solution was performed in ACN mixed with 0.1 M TBAP and 10 mM ferrocene. $Ag/AgNO_3$ in 0.1 M TBAP was used as the reference electrode together with Pt and FTO electrodes for three-electrode cyclic voltammetry between −250 mV and 450 mV at a scan rate of 100 mV s^{-1}.

The surfactant properties for SPEs of substituted PEA were compared with those of a film from crosslinkable monomer without the amine functional end group: PPGDA. Samples were prepared by spin-coating thin electrolyte layers onto FTO substrates. After UV induced polymerization, both samples were rinsed subsequently with ACN and deionized water.

3. Results and discussion

3.1. Characterization of the bifunctional monomer

By comparing the FTIR spectra of substituted and unsubstituted PEA, shown in Fig. 1, it can be seen that new peaks appeared after substitution with the secondary amide group. The peak at wavenumber ~1670 cm^{-1} corresponds to the C=O stretching vibrations, and the vibrations of C=C acrylic double bonds attached to C=O appears at 1620–1680 cm^{-1}.

^1H NMR was also applied before and after methacrylic substitution. In Fig. 2, the peaks appearing at 5.3 and 5.7 ppm after substitution correspond to the metacrylate group (peak 1). Peak 2 at 7.5 ppm is assigned to proton in the amide group. Furthermore, the peaks 3, 4 and 4′ originate from methyl groups at the chain ends under different chemical environments. It can also be seen that peaks at 4′ and 5′ are shifted toward higher chemical shift as compared to those obtained from unsubstituted PEA. This is due to that both $-CH_3$ and $-CH$ groups are less shielded when linked to an $-NH$ group.

Residues of methacrylic acid by-product (shown in Scheme 1) could be detected as two very small peaks with similar intensity at around 5 and 5.5 ppm, originating from the protons from the methacrylic double bond in the methacrylic acid. It was found that the intensity decreased with the increase of filtration time. Thereby, the intensity of these peaks can be used as the evidence of purity of the final product. The yield of monomer synthesis after completely removing the by-product through column filtration and solvent evaporation was approximately 20–25%. Since the novel monomers contain both unsaturated acrylate groups and nucleophilic amine group, there is a possibility for Michael-addition reactions to occur spontaneously. However, Michael addition is thermodynamically controlled and the reaction is commonly catalytic in basic environment. The monomer was stored at low temperature for several months after synthesis, and the NMR spectrum of the monomer after storage was found to be identical to Fig. 2; clearly indicating that the storage conditions were adequate.

The thermal properties of PEA and substituted PEA before and after polymerization are illustrated in DSC thermograms in Fig. 3. When comparing the DSC thermograms of PEA and substituted PEA, it can be seen that the glass transition temperature (T_g) of substituted PEA is lower compared to that of PEA. This can be explained by the enhancement in flexibility of the polymer chains

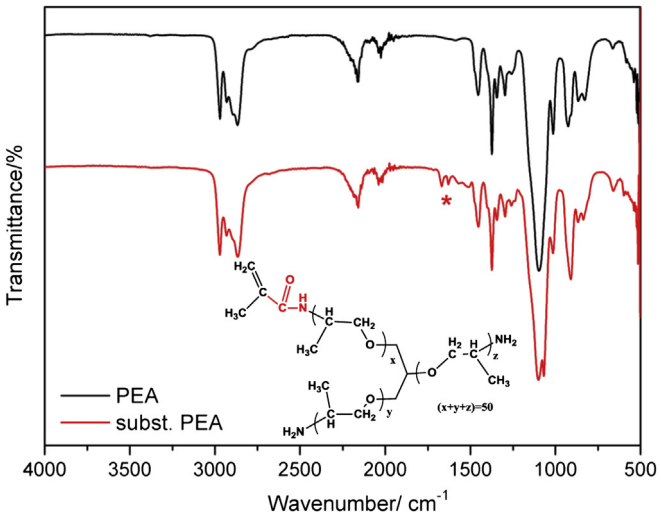

Fig. 1. FTIR spectra of unsubstituted and substituted PEA before polymerization.

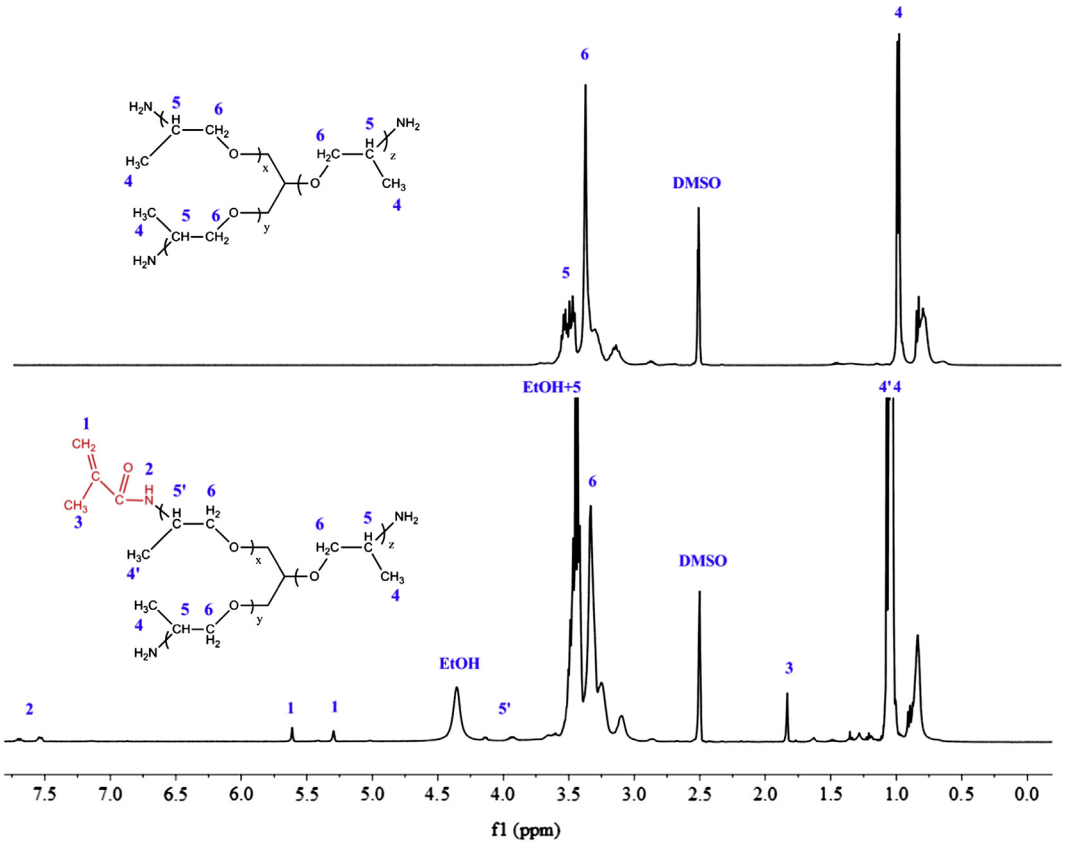

Fig. 2. ^{1}H NMR spectrum of PEA and substituted PEA.

due to the incorporation of methacrylic group at the chain ends. Besides, there is an obvious increase in T_g after polymerizing the mixture of substituted PEA and LiTFSI. This is obviously due to the loss of flexibility in the polymer chains after polymerization and cross-linking, and it therefore requires more energy to promote segmental motions.

3.2. Characterization of the polymer electrolyte

When testing the surfactant property of the electrolyte by rinsing in different solvents, it was found that the thin polymer layer of PPGDA/LiTFSI was directly peeled off from the FTO substrate. In contrast, the one consisting of substituted PEA/LiTFSI remained on the substrate after the same treatment, although it could be partially removed after immersing in the solvent for an extended time. Previous XPS studies on unsubstituted PEA has also showed that the O–H bonding formed between the amine end group and the oxygen sites at electrode surface could facilitate good surface contacts [13,14], and is here confirmed also for polymeric layers.

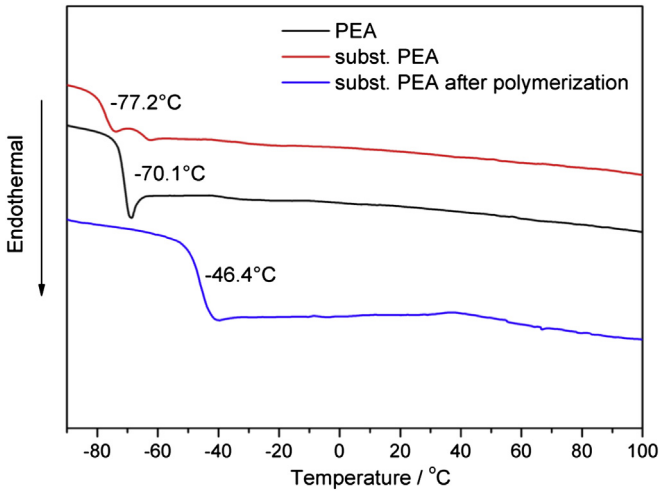

Fig. 3. DSC thermograms and glass-transition temperatures of PEA and substituted PEA.

Fig. 4a and b shows SEM micrographs of the polymer electrolyte coated $LiFePO_4$ electrodes. It can be seen that a thin and conformal polymer layer is deposited successfully onto the rough surface of the 2D composite electrodes, following the 3-dimensional structures of the active material particles. The polymer do not only covers the surface of the nano-particles, but also fills the pores among particles. This is beneficial for promoting the contacts between electrolyte and electrodes, and is a strong indication of the potential use of the electrolyte in 3D-electrode configurations. The thickness of conformal layer is ~1 μm determined from the cross-sectional view in SEM. The thickness was found to be controllable down to the nano-scale depending on the concentration of monomer in the solution applied before polymerization, indicating that the electrolyte could be particularly useful for complex 3D-architectures.

The ability to form pinhole-free polymer electrolyte is critical for 3D-microbattery applications, because pinholes with size in nano-dimension are prone to generate local short-circuits between the electrodes [15,16]. The SPE coating presented here behaves as an electronically insulating layer when deposited onto electronic conductive substrates. The pinhole test was first performed in aqueous solution. Fig. 5 show the voltammetric response of $Fe(CN)_6^{3-}$ in KCl aqueous solution on both uncoated FTO and SPE-coated (3 μm) FTO substrates. As can be seen, there is no active electrochemistry detected after applying the SPE coating onto FTO substrate, indicating

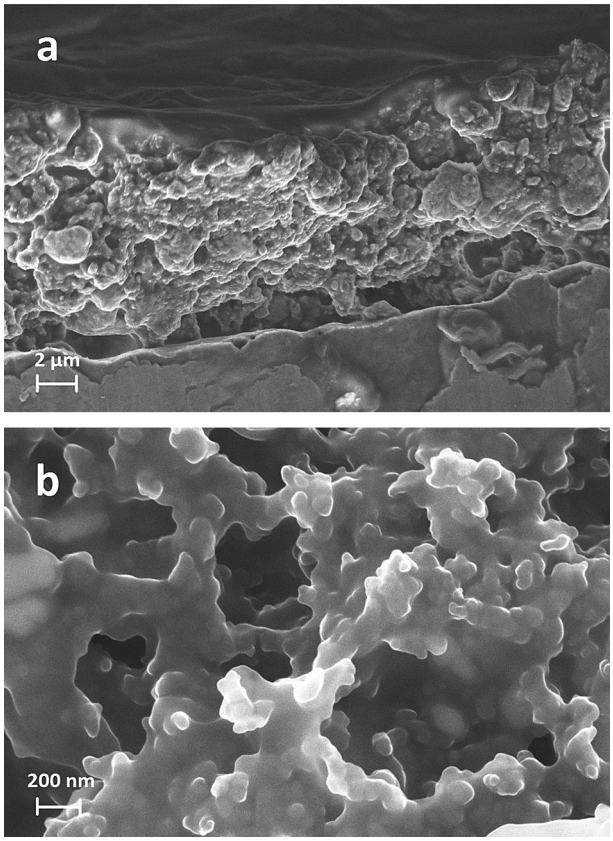

Fig. 4. SEM micrographs of $LiFePO_4$ electrodes coated with SPE: (a) cross-section; (b) surface view.

that the coating is indeed pinhole-free. Although the CV response could be due a limited wettability of the polymer, similar results were obtained in non-aqueous solution using ferrocene as a redox species and ACN as solvent. ACN is less polar and could therefore wet the substituted PEA-based electrolyte film better. A peak at 0.27 V is obvious for uncoated FTO but not observable for a sample coated with a thin (3 μm) polymer layer.

The cyclic voltammograms in Fig. 6 show the electrochemical stability window of both PEA/LiTFSI and an SPE consisting of substituted PEA/LiTFSI. A reduction peak due to the degradation of PEA is clearly seen at around 1.2 V vs. Li^+/Li for the unsubstituted

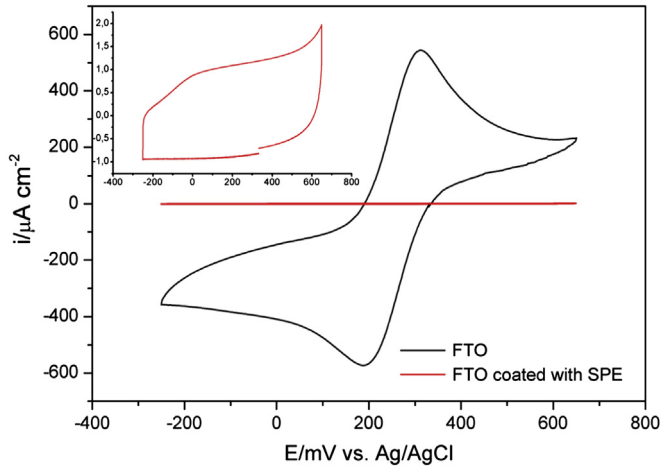

Fig. 5. Voltammetric response of 1 mM $Fe(CN)_6^{3-}$ in 0.1 M KCl at uncoated FTO and SPE-coated FTO substrates with a scan rate of 100 mV s^{-1}.

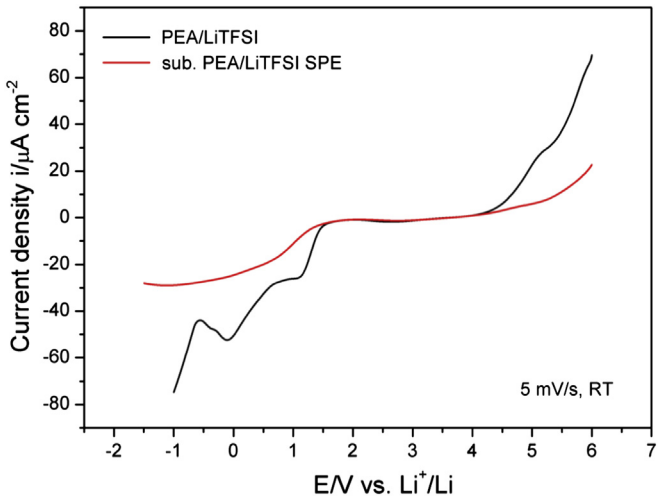

Fig. 6. Cyclic voltammograms of PEA and a substituted PEA-based SPE, both containing LiTFSI salt at a Li:ether oxygen ration 1:20, with a scan rate of 5 mV s^{-1} at room temperature.

sample, while Li plating occurs at approximately 0 V. The substituted PEA/LiTFSI SPE, on the other hand, seem to be rather stable up to 5 V before the oxidation of TFSI anion starts at 5.3 V. However, it is unlikely that the SPE has an electrochemical stability high above 4 V, which is common for polyethers. Furthermore, it is interesting to note that there is no obvious Li plating detected in the low potential region for the SPE sample.

In Fig. 7, the Nyquist plots obtained from EIS measurement can be seen to show two distinct regions: one semicircle at high frequency which corresponds to the bulk properties of the electrolyte, whereas the low frequency 'spur' is related to the interfacial behavior between electrodes and electrolyte [17]. The specific conductivity (σ) of the self-standing SPEs can be calculated from:

$$\sigma = \frac{l}{RA}$$

where l is the thickness of the SPE sample, A is the area of the electrodes, and R is the electrolyte resistance which can also be referred to as bulk resistance.

The ionic conductivity values of the substituted PEA/LiTFSI electrolytes before and after polymerization are listed in Table 1. The SPE display relatively low RT ionic conductivity values, similar to conventional SPEs [18]. Since the ionic conductivity of polymer

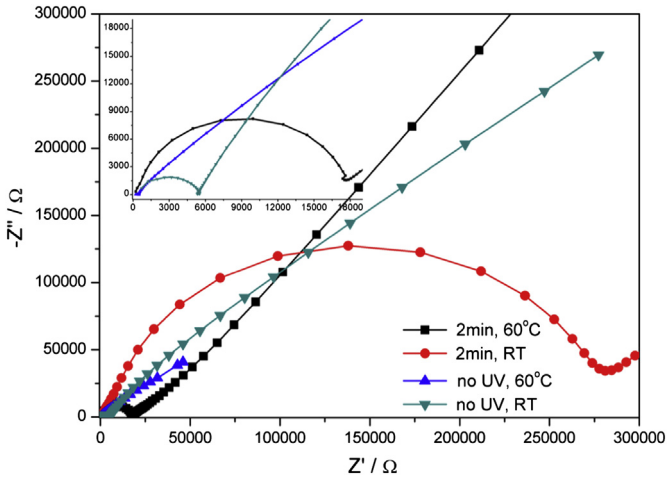

Fig. 7. Nyquist plots of substituted PEA before and after polymerization at RT and 60 °C.

electrolytes increases at elevated temperatures, such systems are especially appealing for high temperature applications. Here, in particular under safety and stability aspects, they appear clearly advantageous over conventional liquid/gel electrolytes. It should also be noted that the samples prepared for ionic conductivity measurement were thick free-standing membranes. By significantly reducing the thickness down to micro- or nano-scales, the Li^+ transport distance within the electrolyte would be much shorter, and thereby the contribution to the internal resistance from the electrolyte would be largely minimized.

Comparing the substituted PEA SPEs to the blended electrolyte based on PEA/PPGDA [10], it can be seen from the data in Table 1 that the novel electrolyte exhibits a lower ionic conductivity about one order in magnitude at 60 °C. This most likely originates from the fact that all monomeric units in the substituted PEA are bonded together covalently, leading to a strengthened network containing less flexible polymer chains. In conclusion, although at the expenses of possessing lower ionic conductivity, SPEs based on the substituted PEA provides enhanced tolerance to most common solvents (*e.g.*, N-Methyl-2-pyrrolidone, acetonitrile, ethanol, cyclohexane and water), and could thereby could be used when subsequently depositing electrode materials in 3DMB whole-cell generation.

3.3. Characterization of $LiFePO_4$/SPE/Li half-cells

The electrochemical performance of thin-film $LiFePO_4$/SPE/Li half-cells using substituted PEA SPE films of ~1 μm was analyzed by galvanostatic cycling at elevated temperature (60 °C; results are shown in Figs. 8 and 9). Fig. 8 displays the cycling performance of the cell within the range of 2.7 V–4.2 V at C/50. It can be seen that the OCV of the battery is around 2.24 V vs. Li^+/Li, which is relatively lower than the OCV of $LiFePO_4$ half-cell using liquid electrolyte (~2.8 V) [19]. This may be explained by the fact that there are few attachment points between the flat Li foil and the roughly-structured composite electrode coated with conformal thin SPE. The charge and discharge plateaus in the first cycle are about 3.5 and 3.4 V, which are expected values. The cycling performance becomes stable in the following cycles, which is also confirmed by a gradual increase in the discharge capacity during first 4 cycles in Fig. 9. This may be attributed to accumulated Li plating at the interface during cycling, introducing more attachment points at the interface. This could at first sight seem contradictory to the lack of observed Li dendrites in the cyclic voltammetry, but these tests were performed on thick self-standing SPE membranes. As the thickness of SPEs is reduced down to micro-scale, the ultra-thin SPE layer is naturally less resistant to Li plating but also to dendrite formation.

In Fig. 9, it can be seen that the discharge capacity of the cells reaches a plateau after first 4 cycles with ~140 mAh g^{-1} for C/50 and ~90 mAh g^{-1} for C/25, which again is likely to be due to a stabilization of the interfacial contacts between the SPE and the Li foil. However, as the accumulation of Li dendrites grows, they can eventually break the ultra-thin SPE layer, and the cell capacity start to fade rapidly after ca 12 cycles for C/25. It was found that better cyclability (at least 30 cycles) could be obtained if the thickness of the SPE layer was increased, thereby preventing the degradation caused by accumulated Li dendrites. However, this improvement is realized at the expenses of losing the conformal nature of the coating and increasing the internal resistance by a thicker SPE. On the other hand, the problems associated with Li dendrites are not likely to occur in whole-cell configurations where the metal Li-foil is replaced by intercalation or alloying anode materials.

Table 1
Ionic conductivity of substituted PEA-based electrolytes before and after polymerization in comparison with PEA/PPGDA blend polymer electrolytes [9]; Li:O = 1:20.

Ionic conductivity σ, S cm^{-1}	RT	60 °C
Subst. PEA before polymerization	9.97×10^{-6}	1.00×10^{-4}
Subst. PEA after polymerization, 2 min	5.28×10^{-7}	8.05×10^{-6}
PEA:PPGDA = 2:1 before polymerization	5.10×10^{-6}	1.10×10^{-4}
PEA:PPGDA = 2:1 after polymerization, 2 min	3.50×10^{-6}	5.80×10^{-5}

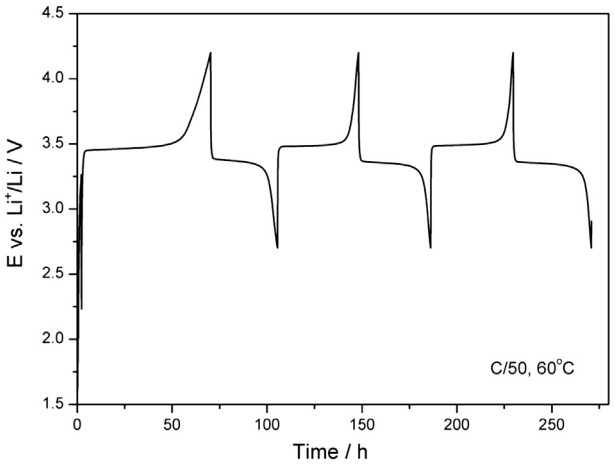

Fig. 8. Galvanostatic cycling of $LiFePO_4$/SPE/Li at 60 °C for C/50.

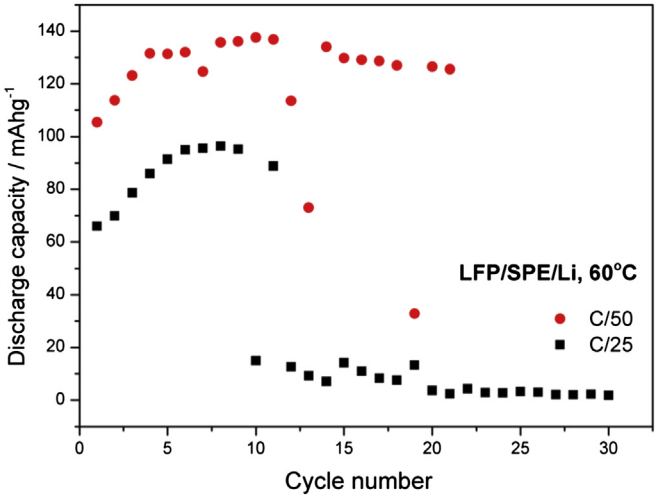

Fig. 9. Discharge capacities of $LiFePO_4$/SPE/Li at 60 °C for C/25 and C/50.

4. Conclusions

In this paper, a new thin solid polymer electrolyte for usage in all-solid-state Li-ion 3D-microbatteries has been investigated. A novel PEA-based monomer was developed, incorporating a polymerizable functionality at some of the oligomer chain ends of the PEA surfactant through methacrylic substitution. FTIR and NMR spectra confirmed a successful substitution of methacrylic group. The ionic conductivity for SPEs generated from the substituted PEA oligomer and LiTFSI was ~8×10^{-6} S cm^{-1} at 60 °C. This can be considered sufficient for usage in 3DMBs, where a conformal and pinhole-free electrolyte medium with ultra-thin thickness is required, rather than high ionic conductivity. SPEs prepared by rapid UV-initiated polymerization exhibited good electrochemical stability above 4 V vs. Li^+/Li and also displayed electrode surface adhesion upon exposure to several organic solvents, where previous electrolytes based on unsubstituted PEA has failed.

Ultra-thin polymer layer in the order of ~1 μm was deposited onto roughly structured $LiFePO_4$ electrodes. SEM micrographs showed that the SPE layer forms a conformal coating onto the nanoparticles and also penetrates into the electrode pores, which is important for usage in 3DMBs. When cycling $LiFePO_4$/SPE/Li half cells, the discharge capacity at 60 °C was comparable to the practical capacity of the $LiFePO_4$ material, but displayed inferior capacity at higher cycling rate. Furthermore, a dramatic decrease in capacity could be seen, probably due to accumulating Li dendrite formation. However, this would be of less importance in 3DMBs, where Li-metal electrodes are not likely to be used.

Acknowledgments

This work has been supported by the STandUP for Energy project.

References

[1] K. Edström, D. Brandell, T. Gustafsson, L. Nyholm, J. Electrochem. Soc. Interface (2011).
[2] T.S. Arthur, D.J. Bates, N. Cirigliano, D.C. Johnson, P. Malati, J.M. Mosby, E. Perre, M.T. Rawls, A.L. Prieto, B. Dunn, MRS Bull. 36 (2011) 523.
[3] K. Dokko, J. Sugaya, H. Nakano, T. Yasukawa, T. Matsue, K. Kanamura, Electrochem. Commun. 9 (2007) 857–862.
[4] H. Kim, R.C.Y. Auyeung, A. Piqué, J. Power Sources 165 (2007) 413–419.
[5] K.B. Lee, L. Lin, J. Microelectromech. Syst. 12 (2003) 840.
[6] M.-S. Park, S.-H. Hyun, S.-C. Nam, S.B. Cho, Electrochim. Acta 53 (2008) 5523–5527.
[7] G. Oltean, L. Nyholm, K. Edström, Electrochim. Acta 56 (2011) 3202–3208.
[8] E. Perre, P.L. Taberna, D. Mazouzi, P. Poizot, T. Gustafsson, K. Edström, P. Simon, J. Mater. Res. 25 (2010) 1485.
[9] S.K. Cheah, E. Perre, M. Rooth, M. Fondell, A. Hårsta, L. Nyholm, M. Boman, T. Gustafsson, J. Lu, P. Simon, K. Edström, Nano Lett. 9 (2009) 3230–3233.
[10] S. Tan, S. Walus, J. Hilborn, T. Gustafsson, D. Brandell, Electrochem. Commun. 12 (2010) 1498–1500.
[11] S. Tan, S. Walus, T. Gustafsson, D. Brandell, Solid State Ionics 198 (2011) 26–31.
[12] S. Tan, E. Perre, T. Gustafsson, D. Brandell, Solid state Ionics, http://dx.doi.org/10.1016/j.ssi.2011.11.005.
[13] C. Sisbandini, D. Brandell, T. Gustafsson, J.O. Thomas, Electrochem. Solid-State Lett. 12 (2009) A99.
[14] C. Sisbandini, D. Brandell, T. Gustafsson, L. Nyholm, J. Electrochem. Soc. 156 (2009) A720.
[15] J.F.M. Oudenhoven, L. Baggetto, P.H.L. Notten, Adv. Energy Mater. (2010) 1–24.
[16] A. Collier, H. Wang, et al., Int. J. Hydrogen Energy 31 (2006) 1838–1854.
[17] P.G. Bruce, Solid State Electrochemistry, Cambridge University Press, 1995.
[18] C. Sequeira, D. Santos, Polymer Electrolytes – Fundamentals and Applications, WP, Cambridge, 2010.
[19] H. Huang, S.-C. Yin, L.F. Nazar, Electrochem. Solid-State Lett. 4 (2001) A170–A172.